Monthly Notices of the ROYAL ASTRONOMICAL SOCIETY
MNRAS **541,** 601–609 (2025)
Advance Access publication 2025 June 25
https://doi.org/10.1093/mnras/staf1025

Circumgalactic medium of quasar host galaxies at $0.4 \leqslant z \leqslant 0.8$ probed by strong Mg II absorption

Paryag Sharma [1]★ Raghunathan Srianand [2] Hum Chand[1] and Labanya Kumar Guha[3]
[1]*Department of Physics and Astronomical Science, Central University of Himachal Pradesh, Dharamshala 176215, India*
[2]*Inter-University Centre for Astronomy and Astrophysics, Post Bag 4, Ganeshkhind, Pune 411 007, India*
[3]*Indian Institute of Astrophysics, II Block, Koramangala, Bengaluru 560 034, India*

Accepted 2025 June 20. Received 2025 June 20; in original form 2025 March 24

ABSTRACT
Using a sample of 166 projected quasar pairs, we investigate the influence of active galactic nuclei on the circumgalactic medium of the quasar host galaxies probed using strong Mg II absorption (i.e. $W_{2796} \geq 1$ Å) at impact parameters (D) <100 kpc. The foreground quasars are restricted to the redshift range $0.4 \leq z \leq 0.8$ and have median bolometric luminosity and stellar mass of $10^{45.1}$ erg s^{-1} and $10^{10.89} M_\odot$, respectively. We report detections of Mg II absorption in 29 cases towards the background quasar and in four cases along the line of sight to the foreground quasars. We do not find any difference in the distribution of W_{2796} and covering fraction (f_c) as a function of D between quasar host galaxies and control sample of normal galaxies. These results are different from what has been reported in the literature, possibly because (i) our sample is restricted to a narrow redshift range, (ii) comparative analysis is carried out after matching the galaxy parameters, (iii) we focus mainly on strong Mg II absorption, and (iv) our sample lacks foreground quasars with high bolometric luminosity (i.e. $L_{bol} > 10^{45.5}$ erg s^{-1}). Future studies probing luminous foreground quasars, preferably at lower impact parameters and higher equivalent width sensitivity, are needed to consolidate our findings.

Key words: galaxies: haloes – quasars: absorption lines – quasars: general.

1 INTRODUCTION

Since quasars were first discovered, their spectra revealed metal absorption lines produced by the intervening gas (Gunn & Peterson 1965; Sandage 1965; Burbidge, Lynds & Burbidge 1966; Burbidge 1967). Subsequent studies established that these metal absorbers were associated with foreground galaxies intersecting the quasar sightlines at low impact parameters (Bahcall & Salpeter 1966; Bahcall & Spitzer 1969; Opher 1974; Roeser 1975; Burbidge et al. 1977; Bahcall 1978; Sargent, Young & Schneider 1982; Bergeron & Stasińska 1986; Steidel & Sargent 1992). This realization has led to the identification of an extended gaseous component surrounding galaxies. Various statistical properties of Mg II absorbers can be reproduced using this gaseous component, referred to as the circumgalactic medium (CGM), around galaxies (see e.g. Petitjean & Bergeron 1990; Srianand & Khare 1994). The CGM also plays a crucial role in galaxy evolution, acting as a reservoir for gas that fuels star formation and accretion processes. Understanding the CGM's properties and its interaction with galactic components is essential for constructing a comprehensive picture of galaxy dynamics (Tumlinson, Peeples & Werk 2017; Fumagalli 2024).

Detecting diffused emission-lines allows direct spatial mapping of the gas and, in principle, provides an alternate probe of the CGM (see e.g. Cantalupo et al. 2014; Martin et al. 2014; Burchett et al. 2021; Das et al. 2024). However, such studies face significant challenges compared to absorption-line studies as the emission measure scales with the square of the gas density (n^2); since the CGM typically has a low hydrogen number density ($n_H \sim 10^{-2}$ cm^{-3} or less), detecting such emission is inherently difficult. Additionally, the surface brightness of CGM emission is extremely faint relative to the sky and detector backgrounds, and surface brightness dimming increases steeply with redshift, further complicating detection. Nevertheless, this limitation is substantially alleviated in the presence of bright quasars, where enhanced ionizing radiation can significantly boost the surface brightness of both resonant and non-resonant line transitions. Recent deep observations have revealed that giant Ly α nebulae are common around luminous quasars at $z \sim 2$–5, demonstrating that the quasar radiation field can illuminate the cool CGM to detectable levels (see e.g. Borisova et al. 2016; Arrigoni Battaia et al. 2018; Fossati et al. 2021).

Observations have shown that the Ly α surface brightness of circum-quasar nebulae correlates with quasar luminosity, indicating that photoionization by the central active galactic nucleus (AGN) plays a major role in powering the emission (Mackenzie et al. 2021). At lower redshifts (i.e. $z \sim 0.4$–1.4), [O II]-emitting circumgalactic nebulae have been detected around UV-luminous quasars, further supporting the presence of dense, metal-enriched gas reservoirs (Dutta et al. 2023; Johnson et al. 2024). In addition, detailed mapping has shown that the morphologies and kinematics of these nebulae arise from a range of processes, including galaxy interactions (Helton et al. 2021; Liu et al. 2024), cool gas accretion (Johnson et al.

★ E-mail: panditparyag@gmail.com

2022), radio jet interaction (e.g. Shukla et al. 2022), and feedback-driven outflows exhibiting elevated velocity dispersions (Zhuoqi et al. 2025). These emission studies provide crucial constraints on the structure, kinematics, and physical conditions of the CGM in quasar host haloes.

In contrast, quasar absorption-line studies offer several advantages. The absorption-line detections are largely independent of redshift and the luminosity of the host galaxy and depends mainly on the signal-to-noise ratio (SNR) achieved for the quasar spectrum. Therefore, by choosing bright enough background sources high sensitivity can be achieved to detect even low column density gas. On the flip side, absorption-line studies provide only projected pencil-beam measurements of gas surface density. In most cases, observations are limited to a single sightline per galaxy due to the rarity of suitably bright background quasars, making it difficult to fully characterize the spatial extent and morphology of the CGM. Therefore, one generally uses statistics based on a sample of quasar–galaxy pairs to characterize the average properties of CGM around galaxies.

Quasar absorption-line studies have yielded profound insights into the nature of CGM (e.g. Nielsen et al. 2013; Mishra et al. 2018; Dutta et al. 2020, 2021, 2023; Joshi et al. 2025). Early efforts to use quasar pairs to probe the CGM of quasars itself were led by Bowen et al. (2006), who demonstrated that strong absorption lines such as Mg II can be detected from the CGM of quasars. These studies were expanded by the Quasars Probing Quasars program (e.g. Hennawi et al. 2006; Prochaska et al. 2013; Lau, Prochaska & Hennawi 2016) and references therein, which focused on $z \gtrsim 2$ quasars and revealed an overdensity around the quasars (see also Jalan, Chand & Srianand 2019, 2021). More recently, studies at lower redshifts, such as Farina et al. (2014) and Johnson, Chen & Mulchaey (2015), showed that quasars at $z \sim 1$ have enhanced Mg II absorption compared to normal galaxies, and that the CGM covering fraction correlates with quasar luminosity. Building on these results, Chen et al. (2023) performed a systematic stacking based analysis of Mg II absorption around quasars in SDSS DR16Q (Lyke et al. 2020), finding a strong decline in absorber incidence with impact parameter and evidence for anisotropy relative to the quasar radiation field.

In this study we adopt the absorption-line technique to probe the CGM because the advent of large-scale spectroscopic surveys like the Sloan Digital Sky Survey (SDSS; Abdurro'uf et al. 2022) and the Dark Energy Spectroscopic Instrument (DESI; DESI Collaboration 2024) has dramatically increased the number of known quasars, providing a significant sample in a narrow redshift range suitable for statistical analysis. In particular, we ask the question whether the properties of CGM, as probed by Mg II absorption, are same for normal galaxies and host galaxies of quasars. Since the samples used in previous studies span a wide range of redshifts and luminosities, comparisons to normal galaxies are not straightforward due to degeneracies inherent in such samples (e.g luminosity dependence versus z-dependence if most of the high-luminosity objects come from high redshifts). To enable a proper comparison between normal galaxies and galaxies hosting a quasar, a controlled investigation is needed, which serves as the main motivation for our work.

This paper is organized as follows: Section 2 describes our sample and absorption line measurements. Section 3 presents our analysis and results, and in Section 4 we present discussion and conclusion of our findings. Throughout this work, we assume a flat Lambda cold dark matter cosmology with $\Omega_m = 0.3$, $\Omega_\Lambda = 0.7$, and $h_0 = 0.7$.

2 SAMPLE AND ABSORPTION LINE MEASUREMENTS

The sample of projected quasar pairs used in this study is sourced from the Sixteenth Data Release of the Sloan Digital Sky Survey (DR16Q; Lyke et al. 2020), comprising 750 414 quasars. Given the signal-to-noise limitations of large survey spectra, we concentrate our analysis on strong intervening Mg II absorbers. We restrict the impact parameter to be less than 100 kpc to focus on the inner regions of the CGM, where strong Mg II absorption is most likely to occur. Beyond this scale, Mg II absorption tends to be significantly weaker with much lower covering factor. Moreover, this limit helps us to ensure that the detected absorption is most likely to be arising from a single galaxy halo, minimizing contamination from neighbouring galaxies or large-scale clustering, though such effects are unlikely in view of the recent underdensity observed around quasars (Shibata et al. 2025). To minimize the effects of redshift evolution in our study, we focus on quasar pairs where the foreground quasar falls within the redshift range $0.4 \leq z \leq 0.8$. The lower redshift limit of $z = 0.4$ ensures that Mg II absorption remains within the optical spectral range, while this redshift interval also corresponds to a regime where the equivalent width versus impact parameter distribution is well sampled for normal galaxies. Therefore, we apply the following criteria to construct our sample:

(i) We first demand that the transverse separation between quasar sightlines at the redshift of the foreground quasar is less than 100 kpc and is satisfied only by 1115 projected quasar pairs.

(ii) We restricted the redshift of the foreground quasar to the range $0.4 \leq z_f \leq 0.8$, reducing the sample to 202 projected pairs.

(iii) A minimum velocity offset of 6000 km s^{-1} is imposed between the redshifts of the foreground and background quasars to reduce the likelihood of quasar pairs being associated (as also used in previous study by Chen et al. 2023). This further reduces the size of our sample to 180 projected quasar pairs.

(iv) To avoid contamination of the Mg II absorption by high-z Lyα forest in the background quasar spectra, we imposed the condition $(1 + z_f) \times 2800 \geq (1 + z_b) \times 1300$, where z_f and z_b are the redshifts of the foreground and background quasars, respectively. After applying this conditions we are left with 149 projected quasar pairs.

One pair, featuring the foreground quasar J083649.46+484150.1 from Bowen et al. (2006), was also included in our sample. Additionally, we performed the same sample selection exercise on the DESI EDR (DESI Collaboration 2024) and identified a total of 16 projected quasar pairs satisfying all the above constraints. We also searched for projected quasar pairs where one quasar is from the DESI sample and the other from the SDSS sample, but did not find any pairs that satisfied our selection criteria. Thus, our final sample consists of 166 quasar pairs.

To start with, we measure the 3σ upper limit of Mg II rest equivalent width (W_{2796}) in the spectrum of the background quasar within $\pm 1500\, kms^{-1}$ with respect to the foreground quasar's redshift, following the procedure described by Churchill et al. (2000). For this purpose, we have used line-free regions after clipping the absorption lines, if present, in the above-mentioned velocity range. Cumulative distribution of the 3σ limiting Mg II rest equivalent width for the full sample is shown in Fig. 1. It is evident from the figure that only 63 per cent (i.e. 105 sightlines) of the background quasar spectra have sufficient SNR so that we can detect Mg II absorption with $W_{2796} \geq 1$ Å at $> 3\sigma$ level. For the statistical analysis of direct detections we use these projected quasar pairs and a limiting threshold W_{2796} of 1 Å.

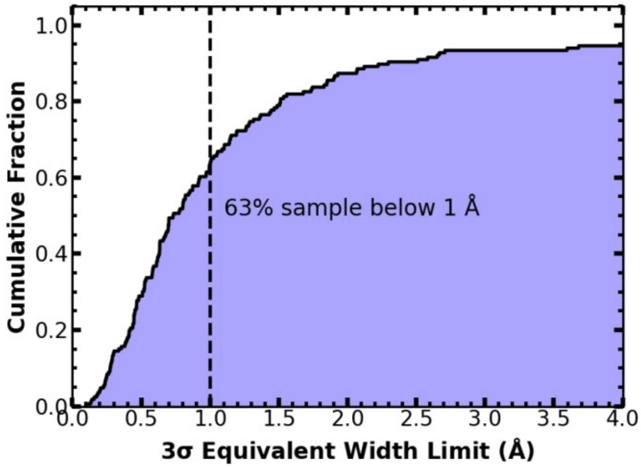

Figure 1. Cumulative distribution of the 3σ limit of W_{2796} in the spectrum of background quasars at the location of the foreground quasars. The vertical dashed line marks the rest equivalent limit of 1Å.

Properties of Mg II absorption are known to depend on the bolometric luminosity (L_{bol}) of the foreground quasars (e.g. Johnson et al. 2015). We have used the bolometric luminosities for SDSS quasar pair from Wu & Shen (2022), and also used their method for estimation of L_{bol} of our the DESI quasars as well. In the top panel of Fig. 2 we compare the bolometric luminosity of foreground quasars in our sample with those from Johnson et al. (2015). It is clearly evident that compared to their sample, quasars in our sample typically probe the low bolometric luminosity range. In particular while studying the luminosity-dependent effects Johnson et al. (2015) defined the low-luminosity objects as the ones with $\log L_{bol}(\mathrm{erg\,s^{-1}}) < 45.5$ (marked with vertical dashed line in the Fig. 2). As can be seen from the figure only 20 per cent of our quasars have L_{bol} in excess of $10^{45.5}$ erg $\mathrm{s^{-1}}$. This is an important factor to remember while comparing our results with that of Johnson et al. (2015). In the bottom panel of Fig. 2 we compare the distribution of L_{bol} between the two samples if we restrict ourselves to $D \leq 100$ kpc and foreground redshift range from 0.4 to 0.8. Clearly, our sample provides a substantial improvement at low redshift and low bolometric luminosity range compared to the sample of Johnson et al. (2015).

We identify Mg II doublet features in the background quasar spectrum within ± 1500 km $\mathrm{s^{-1}}$ of the foreground quasar redshift (as per the criteria in Chen et al. 2023) by visual inspection. These were confirmed when the Mg II doublet ratio is in the allowed range and by the presence of additional associated absorption from species such as Mg I and Fe II. We detected Mg II doublets along 29 background quasar lines of sight within $\pm$ 1500 km $\mathrm{s^{-1}}$ from z_f. Out of these 29 detections, 18 detections have their measured Mg II rest equivalent widths significant at $> 3\sigma$ level and in the remaining cases the measured equivalent widths are at $\sim 2\sigma$–3σ level. In Table 1 we provide the details of the projected quasar pairs, impact parameter (D) at the redshift of the foreground quasar, Mg II rest equivalent width or its 3σ upper limit in case of non-detections, and absorption redshift. For completeness, we also examined quasar pairs with a velocity separation of less than 6000 km $\mathrm{s^{-1}}$. Among 22 such pairs, we detected Mg II absorption in three cases. However, these pairs are excluded from our analysis, as the absorption could originate either from the CGM of the foreground quasar or from the associated absorption of the background quasar. We also searched for Mg II absorption in the spectra of foreground quasars within a 3000 km $\mathrm{s^{-1}}$ window blueward of their redshift to identify any line-of-sight absorption. Mg II absorption is detected in only four out of 166 cases.

Publicly available systemic redshifts of SDSS quasars are known to exhibit systematic biases of $\Delta z/(1+z) \geq 0.002$ (i.e. ≥ 600 km $\mathrm{s^{-1}}$). Hewett & Wild (2010) have improved the accuracy by a factor ~ 20 using Ca II absorption from the host galaxy and low-ionization emission lines. In the SDSS DR16 catalogue, revised redshifts are provided for quasars where systematic corrections were applied; however, in some cases, only visually inspected redshifts are reported, which are less reliable. To ensure consistency and accuracy, we adopted the improved systematic redshifts for foreground quasars provided in Wu & Shen (2022). To obtain accurate absorption redshifts, we utilized `VoigtFit` (Krogager 2018) to simultaneously fit the Mg II 2796, 2803 and Fe II 2600 absorption lines. In cases

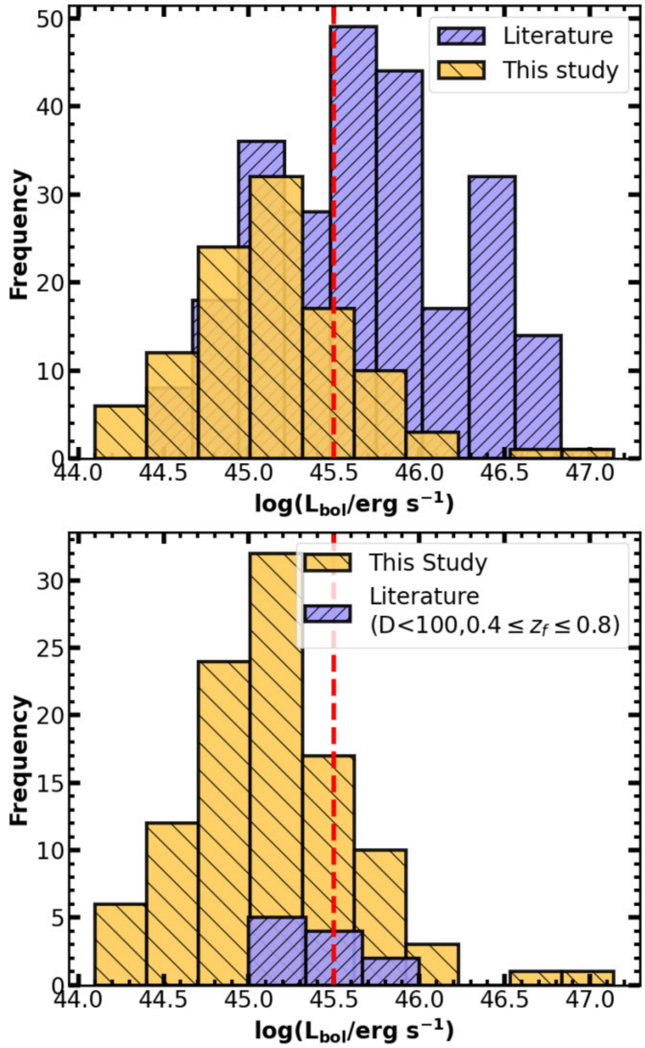

Figure 2. Comparison of the bolometric luminosity of quasars in our sample with the full compiled sample from Johnson et al. (2015), which includes data from Bowen et al. (2006), Farina et al. (2014), and Prochaska, Lau & Hennawi (2014). We label this combined data set as 'Literature' in the figure legend. The top panel shows the comparison with their full sample. The bottom panel focuses on quasars within the same redshift and impact parameter ranges considered in our study. The vertical dashed line marks $log(L_{bol}/\mathrm{erg\,s^{-1}}) = 45.5$, the division between the luminous and low-luminosity quasars used in the literature sample.

Table 1. Table displaying the information about our quasar pair sample. The cases in which there is a detection of Mg II absorption line at the foreground redshift have the equivalent width specified. For cases where the line has not been detected, we provide the 3σ W_{2796} threshold and the error associated with is -1. The entire table consisting of 166 quasar pairs is available online; here we display its structure and contents.

No.	Background quasar	Redshift z_b	Foreground quasar	Redshift z_f	$D_\perp$ (kpc) at z_f	z_{abs}	W_{2796} (Å) Mg II 2796	Err W_{2796} (Å) Mg II 2796
1	J003715.09+055029.2	2.096	J003715.29+055022.7	0.517	44.155	0.517	0.72	0.35
2	J012906.68+004322.9	1.838	J012906.33+004322.0	0.743	38.928	0.742	2.43	1.03
3	J013416.95+330854.5	1.136	J013416.69+330855.9	0.706	25.514	–	0.39	−1
⋮	⋮	⋮	⋮	⋮	⋮	⋮	⋮	⋮

where the SNR was low and simultaneous fitting was not feasible, we fitted only the Mg II lines, selecting one or both depending on the line profiles. To compare the properties of Mg II absorption from the quasar host galaxies in our sample and normal galaxies at $0.4 \leq z \leq 0.8$, we use the data from Nielsen et al. (2013, refer to as MAGIICAT sample) and Huang et al. (2021) for normal galaxies and refer to them collectively as 'galaxy sample'. We note that this galaxy sample comprises a mix of both star-forming and quiescent galaxies. However, due to significant uncertainties in classifying the nature of quasar host galaxies, we do not distinguish between star-forming and quiescent types in our analysis.

In Fig. 3, the top panel illustrates the velocity offsets of the detected absorbers relative to the foreground quasar. The bottom panel of Fig. 3 presents the velocity offset distribution for the galaxy sample within the selected redshift and impact parameter ranges. We performed a Kolmogorov–Smirnov (KS) test between distribution of velocity offset between two samples. The initial analysis yielded a KS statistic of 0.44 with a corresponding p_{null} of 0.002, suggesting a statistically significant difference between the two distributions. However, it is important to consider the potential impact of the quasar's inherent velocity offset, calculated as $\mu = 65.68\ \mathrm{km\,s^{-1}}$, which may originate from systematic uncertainties in obtaining systemic redshift of the foreground quasars. After accounting for this offset, a subsequent KS test returned a statistic of 0.186 with a p_{null} of 0.528. This reduces the statistical dissimilarity to a significant extent. We note that the r.m.s. velocity dispersion of the quasar sample is 135 km s^{-1}, which is smaller than the 188 km s^{-1} measured for the galaxy sample. The latter is also substantially higher than the 84 km s^{-1} reported for a galaxy sample by Huang et al. (2021). This discrepancy could be attributed to differences in sample selection. In Huang et al. (2021), a 'galaxy-first' approach was employed, where galaxies were identified prior to searching for associated Mg II absorption. This method typically yields a lower r.m.s. velocity dispersion. In contrast, our galaxy sample is also based on the MAGIICAT data set, which has less precise galaxy redshifts and incorporates a mixture of both 'galaxy-first' and 'absorption-first' selection strategies. In the latter case, galaxies are identified after detecting absorption features, which increases the likelihood of associating absorbers with bright galaxies in the field. This may introduce a systematic velocity offset. Notably, our quasar sample is conceptually similar to the 'galaxy-first' approach (aside from redshift uncertainties), which could also help explain the relatively lower r.m.s. velocity dispersion compared to our galaxy sample.

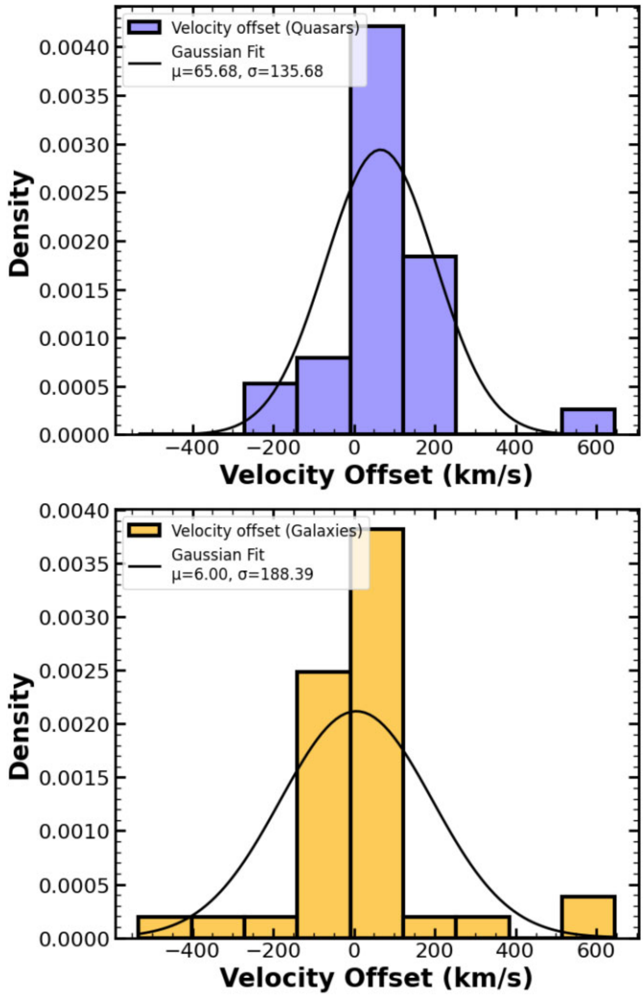

Figure 3. The top panel displays the velocity offset between the redshift of the foreground quasar and the Mg II absorption redshift, highlighting a strong correlation between the two, except mean offset quasar reading. The bottom panel Illustrates the same velocity offset for galaxies with $D < 100$ and $0.4 \leq z \leq 0.8$, providing further context for the observed trends.

3 RESULTS

In this section we summarize our results of comparing properties of Mg II absorption originating from quasar host galaxies and normal galaxies at $0.4 \leq z \leq 0.8$ and at impact parameters $D \leq 100$ kpc.

3.1 Equivalent width versus impact parameter

The rest equivalent width of Mg II absorption is known to show clear anticorrelation with the impact parameter (Bergeron & Boissé 1991) albeit with a large scatter (Chen et al. 2010; Nielsen et al. 2013). This relationship is usually approximated by the log-linear relationship as

$$\log W_{2796}(\text{Å}) = \alpha \times D\ (\text{kpc}) + \beta, \quad (1)$$

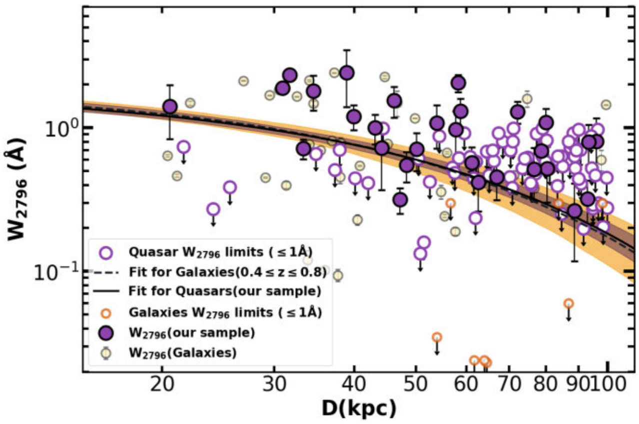

Figure 4. W_{2796} versus impact parameter (D) for foreground quasars. The violet filled circles indicate detections; the open circles with arrows show upper limits. Galaxy detections are shown as faded yellow circles; the upper limits as open orange circles. The solid black line with violet shading shows the quasar fit; the dashed black line with yellow shading shows the galaxy fit over the same redshift range.

Table 2. Comparison of α, β, and σ values for Mg II W_{2796} versus D relation (see e.g. Fig. 4).

Sample ($0.4 \le z \le 0.8$)	α	β	σ
Quasar	-0.010 ± 0.001	0.295 ± 0.039	0.346 ± 0.034
Galaxies	-0.011 ± 0.002	0.315 ± 0.052	0.691 ± 0.075

where β is log W_{2796}(Å) at $D = 0$ kpc and α provides the exponential scale length. We performed the fit among the quasar and galaxy samples following the standard procedure described in Guha et al. (2022)[1] by using the detections as well as upper limits from non-detections, to compare their best-fitting parameters: the slope (α), intercept (β), and intrinsic scatter (σ). The best fit is shown in Fig. 4 and best-fitting parameter values are summarized in Table 2. As can be seen in Table 2, the best-fitting values of α and β for the quasar and galaxy samples are consistent within error bar. However, the best-fitting value of σ among the two sample differs significantly. This difference here can be primarily driven by the range of equivalent widths probed in each sample: the galaxy sample includes both strong and weak absorbers down to $W_{2796} = 0.3$ Å, whereas the quasar sample includes strong absorbers with detection upper limits greater than or equal to 1Å. Therefore, the difference in value of σ obtained for two samples can be attributed to the effect of instrumental sensitivity rather than any differences in the underlying CGM properties. To further quantify this dependence, we performed a test using the full galaxy sample, omitting redshift and impact parameter cuts in order to improve upon the statistics by utilizing a larger sample size. To simulate the effect of reduced sensitivity in the galaxy sample – comparable to that of the quasar sample with a minimum detected W_{2796} of ~ 0.3 Å – we modified the galaxy sample by replacing all detections with $W_{2796} < 0.3$ Å, along with the upper limits, with randomly selected upper limits drawn from the quasar sample. Additionally, we excluded one high value outlier ($W_{2796} > 3$ Å). The best-fitting scatter in this sample is found to be 0.454 ± 0.018, showing a deviation of approximately 6σ compared to its original (higher sensitivity sample) value of 0.740 ± 0.043. The best-fitting values of the slope (α) and intercept (β) exhibit only marginal changes, with their values of -0.011 ± 0.001 and 0.261 ± 0.010, respectively. These remain consistent with the original values of -0.011 ± 0.002 and 0.315 ± 0.052 within the 1σ uncertainty range. These results show that sensitivity limits contribute significantly to the observed scatter and that reducing the sensitivity brings the galaxy sample scatter from 0.740 ± 0.043 to 0.454 ± 0.018, which is closer to the scatter in quasar sample (0.346 ± 0.034). However, a residual difference remains, suggesting additional contributing factors. A forward-modelling approach (e.g. Huang et al. 2021) may better account for these effects and will be explored in future work.

As discussed in Guha, Srianand & Petitjean (2024) the relationship between W_{2796} and impact parameter (D) is sensitive to the distribution of impact parameter probed. For example, inclusion of Ultra-Strong Mg II absorbers and "galaxy on top of quasars" that probe typical impact parameters $\leq$30 kpc makes β values increase by a factor of 1.7, compared to the literature data that usually probe larger impact parameters (see Guha et al. 2022, 2024; Guha & Srianand 2023, 2024). Note that both our quasar and galaxy samples used here have very few sightlines at $D < 20$ kpc. This could explain why our β values are less than the best-fitting values obtained by Guha et al. (2024).

Further, we note that the distribution of the impact parameter D in our quasar sample differs significantly from that of the galaxy sample ($p_{null} = 0$), primarily because the quasar sample includes a larger number of data points at higher impact parameters. To investigate whether this discrepancy biases our results, we resampled the quasar data based on the impact parameter distribution of the galaxy sample, ensuring an equal number of points in each subset. This resampling was performed multiple times. In Fig. 5, we plot the distributions of α and β obtained from these resampled quasar data sets and compare them with the corresponding fit for the galaxy sample (including upper limits) within our redshift range. The medians of the Gaussian fits are found to be approximately equal to the values of α and β obtained for the galaxy sample within measurement uncertainties. This indicates that the similarity observed in the W_{2796} versus D relation between the galaxy and quasar samples is not biased by the differences in their impact parameter distributions.

It was also suggested that at a given impact parameter the measured W_{2796} might depend on the galaxy luminosity (see discussions presented in Guha et al. 2024). Therefore, next we explore whether such a trend is present with respect to the bolometric luminosity of quasars. We also searched for a possible correlation between $log(W_{2796}) - \alpha \times log(D)$ and L_{bol}. We did not find any significant correlation between the two quantities (Spearman Rank correlation: -0.037, p_{null}: 0.704). This implies that the scatter in W_{2796} versus D plot is not driven by the dependence of this relationship on L_{bol}, at least in the sample considered here. It is worth noting that Chen et al. (2023), using stacked spectra, reported a dependence of rest equivalent width on luminosity. However, their higher luminosity sample has log $L_{\rm bol}/{\rm erg\,s^{-1}} \geq 45.66$, with most of the bright quasars coming from high-z range. Lack of such bright quasars in our sample prevents us from any direct comparison with their study.

3.2 Mg II covering fraction

The covering fraction (f_c) is defined as the ratio of number of detections above a given rest equivalent width (W_{2796}) threshold to the total number of sightlines with sufficient sensitivity to detect Mg II absorption at that threshold. Accordingly, our f_c estimates at a chosen W_{2796} threshold include only those sightlines – whether detections

[1]For non-detections, the likelihood integral is computed with a lower bound of $W_{2796} = 0$ Å.

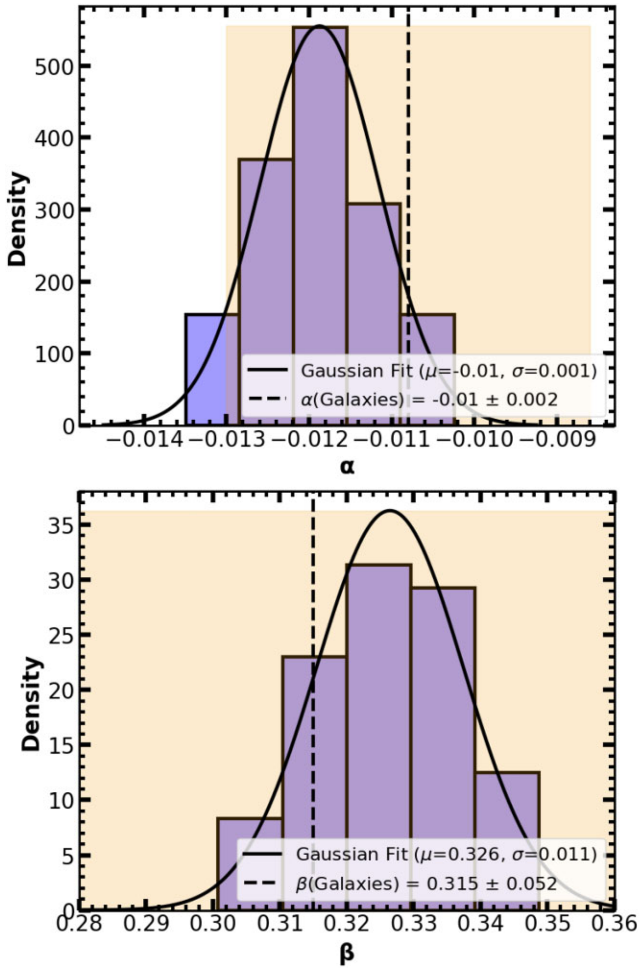

Figure 5. Figure shows the distributions of α (*top panel*) and β(*bottom panel*) for various realizations of control sample of quasars matching in impact parameter of galaxy data with impact parameter tolerance of 10 kpc. The results indicate that both distributions are consistent with each other, suggesting no significant discrepancies in the parameter values despite the imposed selection criteria. The vertical dashed lines represent the α and β values for the galaxy sample, while the shaded region indicates the associated error.

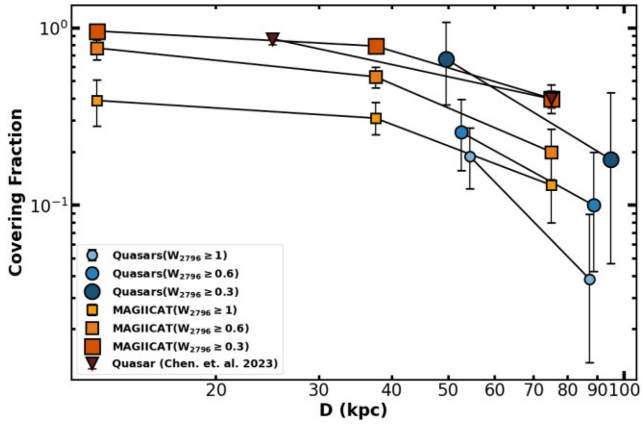

Figure 6. Comparison for the covering fraction of the CGM of galaxies hosting quasar in our sample with that of (i) similar study (i.e. quasar hosting galaxies) by Chen et al. (2023) and (ii) the CGM study of normal galaxies in MAGICAT by Nielsen et al. (2013).

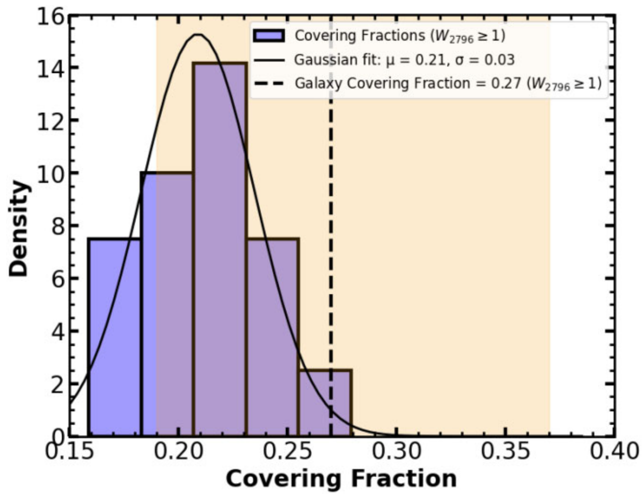

Figure 7. Comparison of the covering fraction distribution of quasars with galaxies, selecting quasars with impact parameters within a matching tolerance of 10 kpc for the galaxy sample, constrained by $D < 100$ kpc and foreground galaxies with redshifts in the range $0.4 \leq z \leq 0.8$. The vertical dashed line shows the covering fraction and the associated error for the galaxy sample with the same range of redshift and impact parameter.

or non-detections – that have an SNR adequate to detect the desired equivalent width at the 3σ level. In Fig. 6, we present the covering fractions of Mg II absorbers for three different threshold of W_{2796} in two impact parameter bins having equal number of sightlines. First, we observe that our sample follows the well-established trend of decreasing covering fraction with increasing impact parameter and rest equivalent width threshold. For comparison we show the results obtained for MAGIICAT galaxies (Nielsen et al. 2013) and results obtained by Chen et al. (2023) for their full sample of galaxies. Our covering fraction measurements are consistent with the literature values. However, to draw a firm conclusion it is necessary to restrict the galaxy sample to the same redshift and impact parameter range as the quasar sample.

To achieve this, as before, we resample the quasar data to match the impact parameter distribution of the galaxy sample. We then calculate the average covering fraction within $D = 100$ kpc. This process is repeated multiple times to generate a distribution of covering fractions. The resulting covering fraction distribution for quasars is presented in Fig. 7, along with the covering fraction for normal galaxies, represented by a vertical black dashed line. The shaded region around this line indicates the corresponding uncertainty. As evident from the figure, the covering fraction for quasar host galaxies remains well within the 1σ uncertainty of the covering fraction observed for normal galaxies.

Johnson et al. (2015) found a strong correlation between the covering fraction and bolometric luminosity. They also observed that the covering fraction measured at a given impact parameter is higher for quasar host galaxies with high luminosities ($\log L_{\rm bol}/$ erg s^{-1} > 45.5) compared to normal galaxies. To explore this, in Fig. 8, we plot W_{2796} as a function of $L_{\rm bol}$ where we have also included 3σ limits for $W_{2796} \geq 1$ Å. To assess the relationship between W_{2796} (including limits) and $L_{\rm bol}$, we applied a Gehan–Wilcoxon-type log-rank test resulting in test statistic of 0.81 and p_{null} of 0.67, indicating no significant dependence between W_{2796} and $L_{\rm bol}$. Next, we divide the sample into two luminosity bins at $\log L_{\rm bol}/\mathrm{erg\,s^{-1}} = 45$. The estimated covering fractions for absorbers with $W_{2796} \geq 1$ Å are also

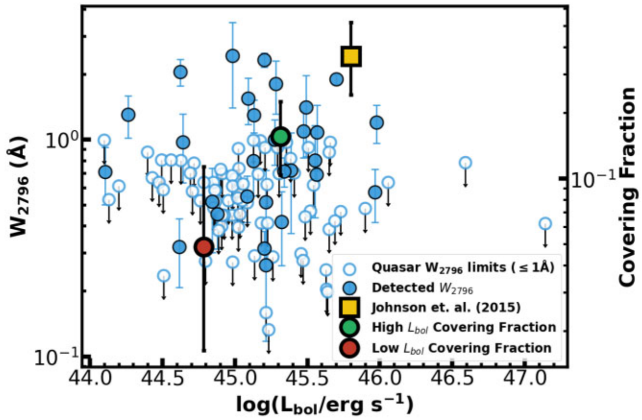

Figure 8. The figure illustrates the variation of W_{2796} with bolometric luminosity for the quasar sample. Overlaid in the right-hand side ordinate are the covering fractions for two luminosity bins and $W_{2796} \geq 1$.

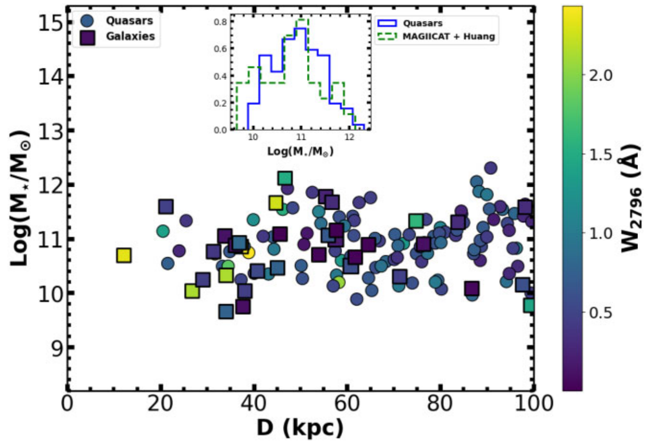

Figure 9. The plot illustrates the variation of stellar mass with the impact parameter, colour-coded by the equivalent width of the detected Mg II absorption line. For quasar host galaxies the stellar mass is calculated using the relation given by Decarli et al. (2010), as given in equation (2).

shown in Fig. 8. We observe a clear increasing trend in covering fraction with increasing $L_{\rm bol}$. Since we consider a restricted range of impact parameters and redshifts, the redshift distributions of the two luminosity bins are consistent with each other, as confirmed by a KS test yielding a p_{null} of 0.45. Similarly, the KS test for the impact parameter distributions results in a p_{null} of 0.33, indicating no significant difference between the two luminosity samples, which can create a bias in the calculation of the covering fraction. Thus, we confirm a weak dependence of the covering fraction on bolometric luminosity. However, we do not find the measured covering fraction for any of the two bins being statistically different from that measured for the galaxy sample.

In Fig. 8, we also include the covering fraction measured for the sample of Johnson et al. (2015) for $D < 100$ but without any restriction on the redshift range. Their measured average luminosity (see Fig. 2) and covering fraction (i.e. $0.36^{+0.15}_{-0.12}$) are higher than those obtained for our sample ($0.11^{+0.04}_{-0.03}$). This once again indicates the increase in covering fraction with increasing bolometric luminosity. Note that the sample of Johnson et al. (2015) covers a wider redshift range and any dependence of f_c on z could affect our interpretation of this result. Also the covering fraction for the galaxy population (i.e $0.27^{+0.10}_{-0.08}$) is not significantly different than what is obtained for the sample of Johnson et al. (2015). Thus, our study indicates the need for a detailed investigation of these issues with larger samples well matched in luminosity, impact parameter, and redshift distribution between normal galaxies and quasar host galaxies.

3.3 Influence of stellar mass

It is well documented in the literature that W_{2796} versus D as well as f_c versus D relationships depend on the stellar mass of the galaxy (see for example, Lan 2020). So it is important to check how the stellar mass distribution of quasar host galaxies and normal galaxies used in this work compare with each other. In Fig. 9, we plot stellar mass versus impact parameter for both the sample. This figure also compares the histogram distribution of stellar masses for both the samples. For the galaxy sample, we calculated galaxy stellar masses only for cases where photometry was available in SDSS DR17 (Abdurro'uf et al. 2022) or DECaLS (Decarli et al. 2010) using the method described in Guha et al. (2022). For quasars, the stellar mass was estimated using the empirical relation between black hole mass and host galaxy stellar mass from Decarli et al. (2010), based on 96 quasars over redshifts 0.07–2.74, as

$$\log \frac{M_{\rm BH}}{M_{\rm host}} = \left(0.28 \pm 0.06\right) z \; - \; \left(2.91 \pm 0.06\right). \tag{2}$$

Here, M_{host} represents the stellar mass, while M_{BH} denotes the black hole mass. For SDSS quasars, M_{BH} values were obtained from the catalogue of Wu & Shen (2022). For quasars from the DESI EDR, we applied the same methodology as described in their work to derive M_{BH}, ensuring consistency in stellar mass estimation. As can be seen from Fig. 9, the stellar mass distributions are nearly same. The median stellar mass for the quasar sample is found to be $10^{10.89} M_\odot$, whereas for the galaxy sample, it is $10^{10.86} M_\odot$. To statistically compare these distributions, we performed KS test, which resulted in a KS statistic of 0.170 and a p_{null} of 0.341. Given the high p_{null}, we conclude that there is no significant difference between the two distributions. This result indicates that quasars in our sample reside in host galaxies that are not significantly more massive than the general galaxy population. Therefore, we can conclude that the similarity of the dependence of f_c and W_{2796} on D for both the samples is not influenced by a possible difference in the stellar mass distribution.

3.4 Line-of-sight velocity difference

Johnson et al. (2015) indicated that the velocity offset between the systemic redshift of the quasar and Mg II absorption redshift has large spread compared to what has been found between galaxies and Mg II absorption. We have already noticed that in our redshift and stellar mass matched samples apart from a small offset the distribution is not statistically distinguishable between galaxies and quasar host galaxies. Here, we explore a possible correlation between the bolometric luminosity and line-of-sight velocity difference in our quasar sample. In Fig. 10, we present the velocity offset between the foreground quasar redshift and its bolometric luminosity. Our analysis reveals no significant correlation between these two quantities (Spearman Rank Correlation: −0.009, p_{null} : 0.963). Thus, within our sample, we find no clear evidence that the gas kinematics along the line of sight is influenced by the bolometric luminosity of quasars. The apparent discrepancy with Johnson et al. (2015) may stem from their inclusion of absorption complexes – 6 out of 73 total absorbers exhibit average velocity offsets of 721 km s^{-1} – where multiple Mg II components are treated as distinct systems. This treatment

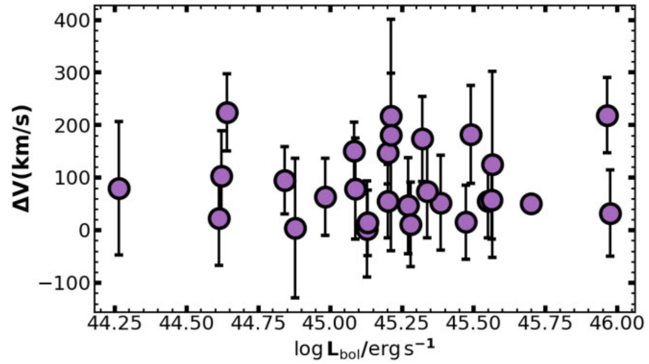

Figure 10. The figure presents the absolute velocity difference between the foreground quasar redshift and the absorber redshift as a function of the bolometric luminosity of the foreground quasar.

contributes to the larger scatter in velocity offsets reported in their study. In contrast, our sample contains no such complexes, and we focus exclusively on strong Mg II systems, which are more likely to originate from regions closer to the galactic centre.

4 DISCUSSION AND CONCLUSION

It is now well established that the CGM consisting of metal-enriched diffuse gas is a crucial component of a galaxy. The CGM serves as a reservoir of gas that regulates star formation and accretion processes. The properties of CGM are probed either through absorption lines detected in the spectra of background quasars or through the detection of diffuse emission. What is the influence of the central AGN on the properties of CGM? This is an important question to address (see Farina et al. 2014; Johnson et al. 2015; Chen et al. 2023, for using Mg II absorption as a tool). These studies have indicated that rest equivalent width of Mg II absorption and its detection rate (or covering fraction) tend to be higher around AGN host galaxies compared to the normal galaxies. It is also well documented that the correlation between W_{2796} and impact parameter has a large scatter and may depend on host galaxy properties such as (i) stellar mass, (ii) luminosity and (iii) redshift etc. Therefore, it is important to probe the influence of quasars using samples that are well matched in various properties of galaxies and impact parameter distribution. This forms the main motivation of this work.

Here, we have utilized a sample of well selected 166 closely spaced quasar pairs, to probe the CGM of quasar hosting galaxies in comparison to the sample of the CGM of normal galaxies in redshift range of $0.4 \leq z \leq 0.8$ and impact parameter range of 20–100 kpc (Section 2). Based on the typical SNR achieved in the SDSS spectra, we mainly focus on systems having $W_{2796} \geq 1$Å. As described in Section 2, our comparison galaxy sample is an amalgamation of MAGICAT (Nielsen et al. 2013) and Huang et al. (2021) sample, matching both in redshift as well as in D. Our main result is that both W_{2796} versus impact parameter (D) distribution and covering fraction (f_c) versus D distribution are statistically similar among the normal galaxies and quasar host galaxies in the aforementioned redshift and impact parameter ranges. We ensured that our results are not biased by the different impact parameter distribution of the two samples. In addition, the stellar mass distributions used for the galaxy sample and quasar host sample are statically similar (e.g. Fig. 9), precluding any bias due to stellar mass dependence. A recent study by Shibata et al. (2025) found that the mean local galaxy density around quasars is ∼ 11–20 per cent lower than that around matched galaxies on scales of 0.3–0.7 pMpc. Although their analysis probes larger scales, this suggests that clustering does not significantly influence the absorbers in our study, supporting the interpretation that our results are independent of large-scale environmental effects.

Splitting our sample into two bolometric luminosity bins we do see a weak dependence of f_c on luminosity, however no correlation was present between the bolometric luminosity and W_{2796}. This appears to be inconsistent with the result of Johnson et al. (2015), who have reported enhanced W_{2796} and f_c for luminous quasar host galaxies compared to low-luminosity quasars and inactive galaxies. However, it may be noted that quasars in our sample typically probe the low bolometric luminosity end of the quasar sample studied by Johnson et al. (2015) and their sample probes a much wider redshift and impact parameter ranges which make direct comparison inappropriate. Moreover to confirm the strong trend in f_c with L_{bol} we need to include sample of high-luminosity quasars over the same redshift range to our sample. This will alleviate the redshift evolution effects influencing the result. It is also important to extend our analysis to lower rest equivalent width limits to see whether the discrepancy is related to us mainly focusing on $W_{2796} \geq 1$ Å absorbers. This can be done by freshly obtaining higher SNR spectra of quasars in our sample.

Similarly, the study by Chen et al. (2023), used large sample over full redshift range probed by SDSS to stack the background spectrum at foreground quasar redshift and showed that the W_{2796} is relatively higher in comparison to W_{2796} from CGM of normal galaxies. It will be important to revisit their analysis with a redshift and impact parameter matched samples of quasar host galaxies and normal galaxies in a restricted redshift range. Chen et al. (2023) have also noticed that detection probability of Mg II absorption along the line of sight is less than that along the transverse direction. We confirm this result in our analysis as well. Interestingly, in the case of normal galaxies the values of W_{2796} as well as f_c is found to increase with decreasing impact parameter (see for example, Guha et al. 2024). Therefore we expect both the quantities to be higher along the foreground quasar line of sight (probing also at low impact parameters) compared to what we find in the transverse direction (probing at higher impact parameters). In addition, one expects contribution of associated Mg II absorption also to be present along the line of sight. Therefore, less detection of Mg II absorption along the line of sight may be related to anisotropy either in the radiation field or matter distribution in the case of quasar host galaxies (see for example, Jalan et al. 2019). Therefore, our finding of similarity in the CGM properties over the impact parameter range 20–100 kpc is intriguing. As mentioned before, we do not have many lines of sight with impact parameter < 50 kpc. It will be important to construct such a sample to confirm the presence of anisotropy in the case of quasars.

Johnson et al. (2015) have also reported an increase in the velocity offset between the quasar host galaxy and absorption redshift with bolometric luminosity. This was also considered as one of the indications of influence of the quasar on the CGM. However, we do not find the scatter in the velocity offset values to increase with increasing luminosity of quasar host galaxies (see e.g. Fig. 8). One possible explanation for the larger velocity offsets reported in Johnson et al. (2015) could be the presence of multiple absorption complexes within their sample. However, this appears unlikely, as only six out of the 73 absorbers are associated with such complexes, and their exclusion reduce r.m.s of the velocity offset only from 496 to 465 km s^{-1}. It is therefore plausible that other factors, such as larger impact parameters, higher quasar host galaxy luminosities, and higher redshift range, may partially account for the discrepancy.

To conclude, our detailed analysis based on a sample of 166 quasars in comparison with a redshift and impact parameter matched control sample of normal galaxies shows no significant difference in the W_{2796}–D and f_c–D distributions among them, indicating that low-luminosity quasars (i.e. mostly $L_{bol} \leq 10^{45}$ erg s^{-1}) do not substantially alter the CGM properties of the host galaxies. For further progress, future studies should focus on observing sightlines selected in a 'galaxy-first' manner, using large samples to enable more accurate comparisons with quasar host galaxies. In parallel, CGM studies of quasar hosts can be improved by targeting (i) luminous quasars, (ii) high SNR data to detect low W_{2796} values, (iii) high spectral resolution to probe detailed kinematics, and (iv) a range of impact parameters (including $D < 50$ kpc as well) by carrying out controlled analysis similar to our study here.

ACKNOWLEDGEMENTS

We thank the anonymous referee for constructive comments and suggestions that helped improve the clarity and quality of this manuscript. The research of PS is supported by the University Grants Commission (UGC), Government of India, under the UGC-JRF scheme (Ref. No.: 221610014755). HC and PS express their gratitude to the Inter-University Centre for Astronomy and Astrophysics (IUCAA) for their hospitality and the provision of High-Performance Computing (HPC) facilities under the IUCAA Associate Programme. We also thank Sowgat Muzahid and Sayak Dutta for their valuable discussions during this project. Additionally, we acknowledge the assistance of AI tools, specifically OpenAI's ChatGPT, for aiding in writing and code development, and Grammarly for enhancing the text's clarity and correctness.

DATA AVAILABILITY

The data used in this study are publicly available in the DESI-EDR, and SDSS DR16 Data Release.

REFERENCES

Abdurro'uf et al., 2022, ApJS, 259, 35
Arrigoni Battaia F., Prochaska J. X., Hennawi J. F., Obreja A., Buck T., Cantalupo S., Dutton A. A., Macciò A. V., 2018, MNRAS, 473, 3907
Bahcall J. N., 1978, Phys. Scr, 17, 229
Bahcall J. N., Salpeter E. E., 1966, ApJ, 144, 847
Bahcall J. N., Spitzer Jr L., 1969, ApJ, 156, L63
Bergeron J., Boissé P., 1991, A&A, 243, 344
Bergeron J., Stasińska G., 1986, A&A, 169, 1
Borisova E. et al., 2016, ApJ, 831, 39
Bowen D. V. et al., 2006, ApJ, 645, L105
Burbidge E. M., 1967, ARA&A, 5, 399
Burbidge E. M., Lynds C. R., Burbidge G. R., 1966, ApJ, 144, 447
Burbidge G., O'Dell S. L., Roberts D. H., Smith H. E., 1977, ApJ, 218, 33
Burchett J. N., Rubin K. H. R., Prochaska J. X., Coil A. L., Vaught R. R., Hennawi J. F., 2021, ApJ, 909, 151
Cantalupo S., Arrigoni-Battaia F., Prochaska J. X., Hennawi J. F., Madau P., 2014, Nature, 506, 63
Chen H.-W., Helsby J. E., Gauthier J.-R., Shectman S. A., Thompson I. B., Tinker J. L., 2010, ApJ, 714, 1521
Chen Z.-F., Qin H.-C., Cai J.-T., Zhou Y.-T., Chen Z.-G., Pang T.-T., Wang Z.-W., Cheng K.-F., 2023, ApJS, 265, 46
Churchill C. W., Mellon R. R., Charlton J. C., Jannuzi B. T., Kirhakos S., Steidel C. C., Schneider D. P., 2000, ApJ, 543, 577
DESI Collaboration, 2024, AJ, 168, 58
Das S. et al., 2024, MNRAS, 527, 10358
Decarli R., Falomo R., Treves A., Labita M., Kotilainen J. K., Scarpa R., 2010, MNRAS, 402, 2453
Dutta R. et al., 2020, MNRAS, 499, 5022
Dutta R. et al., 2021, MNRAS, 508, 4573
Dutta R. et al., 2023, MNRAS, 522, 535
Farina E. P., Falomo R., Scarpa R., Decarli R., Treves A., Kotilainen J. K., 2014, MNRAS, 441, 886
Fossati M. et al., 2021, MNRAS, 503, 3044
Fumagalli M., 2024, The Circum-Galactic Medium Across Cosmic Time: An Observational and Modeling Challenge: Saas-Fee Advanced Course 52,
Guha L. K., Srianand R., 2023, MNRAS, 519, 3319
Guha L. K., Srianand R., 2024, MNRAS, 532, 3056
Guha L. K., Srianand R., Dutta R., Joshi R., Noterdaeme P., Petitjean P., 2022, MNRAS, 513, 3836
Guha L. K., Srianand R., Petitjean P., 2024, MNRAS, 527, 5075
Gunn J. E., Peterson B. A., 1965, ApJ, 142, 1633
Helton J. M., Johnson S. D., Greene J. E., Chen H.-W., 2021, MNRAS, 505, 5497
Hennawi J. F. et al., 2006, ApJ, 651, 61
Hewett P. C., Wild V., 2010, MNRAS, 405, 2302
Huang Y.-H., Chen H.-W., Shectman S. A., Johnson S. D., Zahedy F. S., Helsby J. E., Gauthier J.-R., Thompson I. B., 2021, MNRAS, 502, 4743
Jalan P., Chand H., Srianand R., 2019, ApJ, 884, 151
Jalan P., Chand H., Srianand R., 2021, MNRAS, 505, 689
Johnson S. D., Chen H.-W., Mulchaey J. S., 2015, MNRAS, 452, 2553
Johnson S. D. et al., 2022, ApJ, 940, L40
Johnson S. D. et al., 2024, ApJ, 966, 218
Joshi R., Das S., Fumagalli M., Fossati M., Péroux C., Chaudhary R., Yesuf H. M., Ho L. C., 2025, A&A, 695, A206
Krogager J.-K., 2018, preprint (arXiv:1803.01187)
Lan T.-W., 2020, ApJ, 897, 97
Lau M. W., Prochaska J. X., Hennawi J. F., 2016, ApJS, 226, 25
Liu Z. et al., 2024, MNRAS, 527, 5429
Lyke B. W. et al., 2020, ApJS, 250, 8
Mackenzie R. et al., 2021, MNRAS, 502, 494
Martin D. C., Chang D., Matuszewski M., Morrissey P., Rahman S., Moore A., Steidel C. C., 2014, ApJ, 786, 106
Mishra S., Chand H., Krishna G., Joshi R., Shchekinov Y. A., Fatkhullin T. A., 2018, MNRAS, 473, 5154
Nielsen N. M., Churchill C. W., Kacprzak G. G., Murphy M. T., 2013, ApJ, 776, 114
Opher R., 1974, Nature, 250, 310
Petitjean P., Bergeron J., 1990, A&A, 231, 309
Prochaska J. X. et al., 2013, ApJ, 776, 136
Prochaska J. X., Lau M. W., Hennawi J. F., 2014, ApJ, 796, 140
Roeser H. J., 1975, A&A, 45, 329
Sandage A., 1965, ApJ, 141, 1560
Sargent W. L. W., Young P., Schneider D. P., 1982, ApJ, 256, 374
Shibata K., Nagao T., Uchiyama H., Kubo M., Toba Y., Omori K. C., Kawaguchi T., Suzuki Y., 2025, preprint (arXiv:2505.04259)
Shukla G., Srianand R., Gupta N., Petitjean P., Baker A. J., Krogager J.-K., Noterdaeme P., 2022, MNRAS, 510, 786
Srianand R., Khare P., 1994, ApJ, 428, 82
Steidel C. C., Sargent W. L. W., 1992, ApJS, 80, 1
Tumlinson J., Peeples M. S., Werk J. K., 2017, ARA&A, 55, 389
Wu Q., Shen Y., 2022, ApJS, 263, 42
Will Liu Z. et al., 2025, ApJ, 984, 140

SUPPORTING INFORMATION

Supplementary data are available at *MNRAS* online.

suppl_data

Please note: Oxford University Press is not responsible for the content or functionality of any supporting materials supplied by the authors. Any queries (other than missing material) should be directed to the corresponding author for the article.

This paper has been typeset from a TEX/LATEX file prepared by the author.